

## Supplementary Information

### Phytic Acid Etched Ni/Fe Nanostructures Based Flexible Network as a High-Performance Wearable Hybrid Energy Storage Device

Panpan Li,<sup>a, b</sup> Zhaoyu Jin,<sup>b</sup> and Dan Xiao<sup>b, \*</sup>

**Table S1.** Composition of the coating solution for depositing NiZn alloy and Fe.

Coating NiZn		Coating Fe	
<b>NiSO<sub>4</sub>·7H<sub>2</sub>O (g L<sup>-1</sup>)</b>	120	<b>FeSO<sub>4</sub>·7H<sub>2</sub>O (g L<sup>-1</sup>)</b>	250
<b>ZnSO<sub>4</sub>·7H<sub>2</sub>O (g L<sup>-1</sup>)</b>	31.2		
<b>Na<sub>2</sub>SO<sub>4</sub> (g L<sup>-1</sup>)</b>	40	<b>(NH<sub>4</sub>)<sub>2</sub>SO<sub>4</sub> (g L<sup>-1</sup>)</b>	120
<b>H<sub>3</sub>BO<sub>3</sub> (g L<sup>-1</sup>)</b>	30		

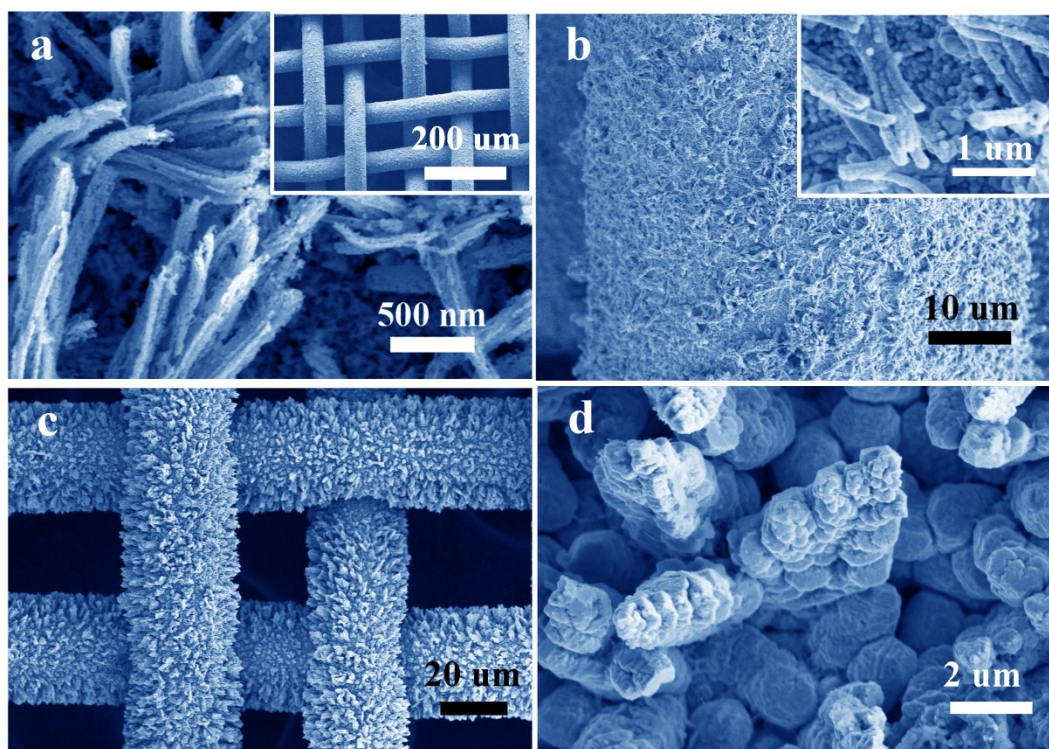


**Fig. S1** SEM images of Cu nanowires (a), 3D-NA/NiZn (b) and 3D-NA/NiZn-phytate (c, d).

As shown in Fig. S1a, Cu nanowires are in-situ grown on Cu network with the diameter of  $\sim 100$  nm by the redox process of  $\text{Na}_2\text{O}_2$  and  $\text{NaBH}_4$ . It is noted that the loose and rich-porous structures are distributed on the wheat-like Cu nanowires from the high magnification (Fig. S1a), which is coincident with the results of the previous work.<sup>1,2</sup> Fig. S1b demonstrates the alloy layer is coated on 3D-NA substrate remaining the shape of Cu nanowires. Then, the obtained 3D-NA/NiZn electrode is followed treated with 0.25 M phytic acid for 5 min. After Zn moiety is mostly dissolved in the phytic acid solution, the appearance of electrode shows a scaly structure as indicated in Fig. S1c and d.

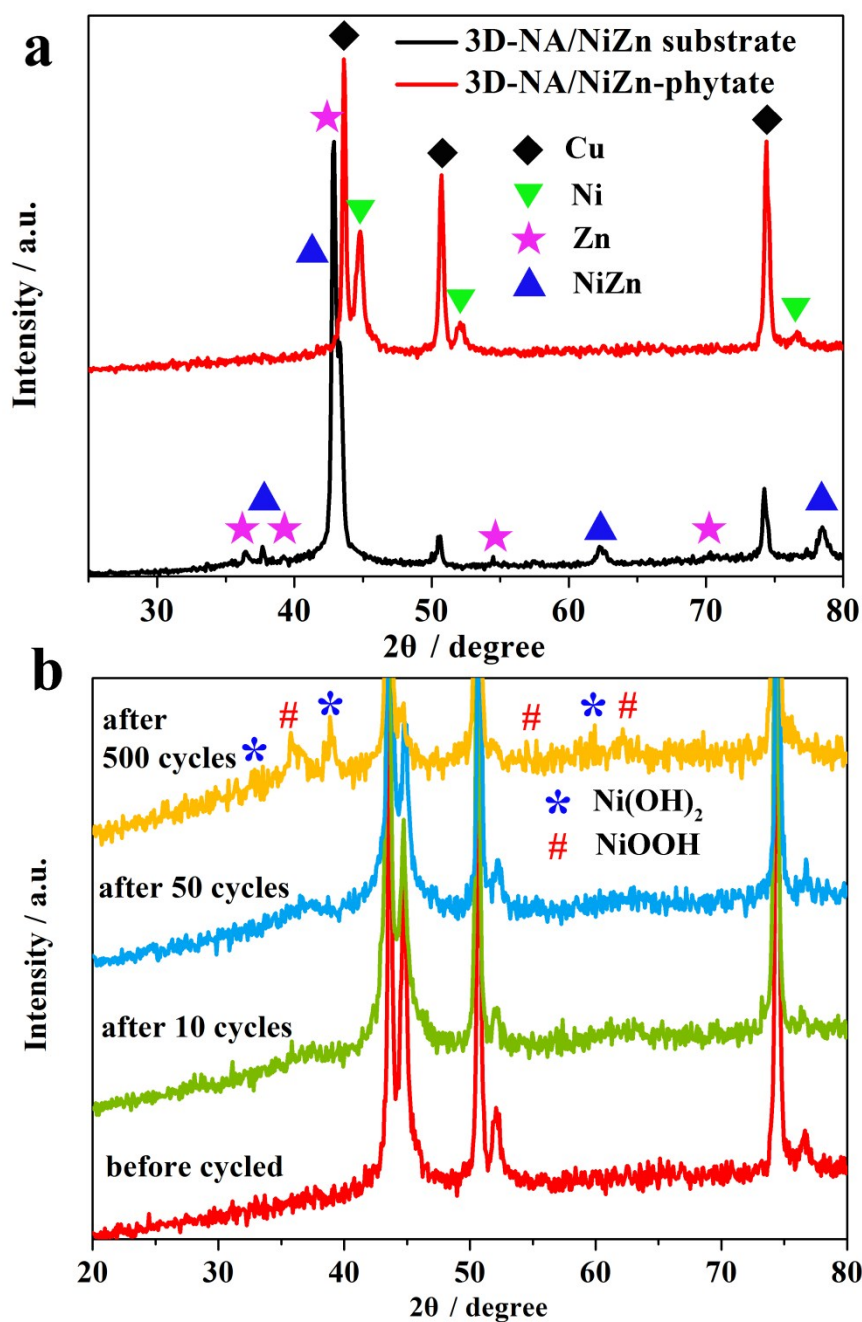


**Fig. S2** XRD patterns of 3D-NA/NiZn substrate (a) and 3D-NA/NiZn-phytate before (a) and after cycled (b).

It is proved that the NiZn alloy is successfully deposited on the 3D-NA from the XRD patterns in Fig. S2a, where peaks marked with  $\blacklozenge$ ,  $\star$  and  $\blacktriangle$  are assigned to Cu, Zn and NiZn alloy according to JCPDS file#70-3039, JCPDS file#04-0831 and JCPDS file#65-5310, respectively. On the contrary, as for 3D-NA/NiZn-Phytate, it is revealed that three new peaks belonging to Ni (marked with  $\blacktriangledown$ , JCPDS file#70-0989) appear, peaks of Cu substrate are enhanced and the peaks of Zn moiety and NiZn alloy disappear.



**Table S2** The quantitative analysis of elements on the surface of 3D-NA/NiZn-phytate before and after 500, 1000 and 1500 cycles.

<b>Elements</b>	<b>before cycled (C<sup>a</sup>/%)</b>	<b>after 500 cycles (C/%)</b>	<b>after 1000 cycles (C/%)</b>	<b>after 1500 cycles (C/%)</b>
<b>Cu</b>	36.38	40.30	42.52	44.00
<b>Zn</b>	34.93	20.50	12.80	12.30
<b>Ni</b>	12.78	18.20	24.04	22.95
<b>O</b>	12.68	20.60	20.42	20.50
<b>P</b>	3.26	0.38	0.32	0.27

<sup>a</sup>C: the abbreviation of mass concentration.

Furthermore, XRF analysis of 3D-NA/NiZn-Phytate also determines that the electrode surface is mainly composed of O, Cu, Ni, Zn, C and P. We can notice that Zn content gradually drops with increasing the cycling numbers, implying the part of Zn moiety is etched away in the alkaline electrolyte. Though Zn content shows the downward trend, it almost maintains at a stable value after 1000 cycles.

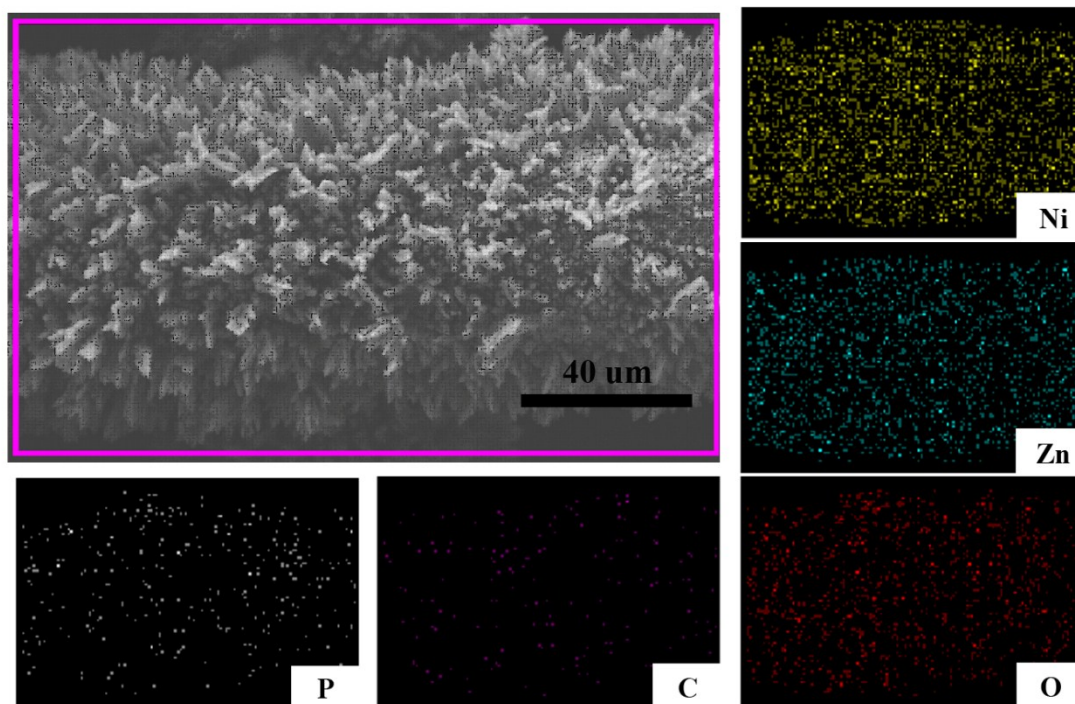


**Fig. S3** EDS element mapping images of Ni, Zn, O, P and C on the surface of 3D-NA/NiZn-phytate.

Additionally, EDS element mapping images are illustrated in Fig. S3, revealing the elements (Ni, Zn, O, P and C) are well distributed on the electrode surface. As we can see, Ni, Zn, O, C and P elements are uniformly dispersed on the surface of electrode. Moreover, the survey scan XPS (Fig. S4) indicates the element composition of 3D-NA/NiZn-Phytate surface is consistent with the result of XRF.

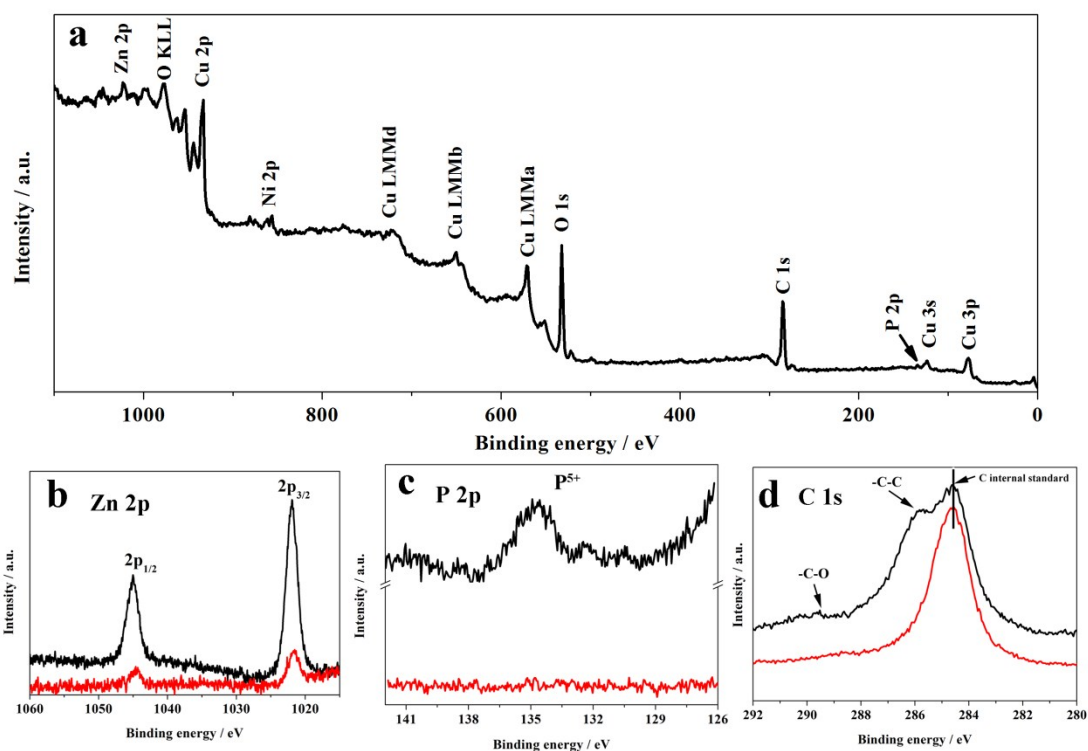


**Fig. S4** survey scan XPS of 3D-NA/NiZn-phytate before cycled (a) and the comparison of Zn 2p (b), P 2p (c) and C 1s (d) before (black curves) and after (red curves) 1000 cycles.

Then, Zn 2p, P 2p and C 1s spectra (Fig. S4b-d) are also remarkably varied. Specifically, there is a dramatic decrease of density observed from Zn 2p of 3D-NA/NiZn-phytate before and after cycled. P 2p spectrum, the -C-C and -C-O peaks of C 1s assigned to the metal-phytate compounds are almost vanished, implying the structure transformation of active materials. These results all confirm the transformation of materials on the electrode surface.

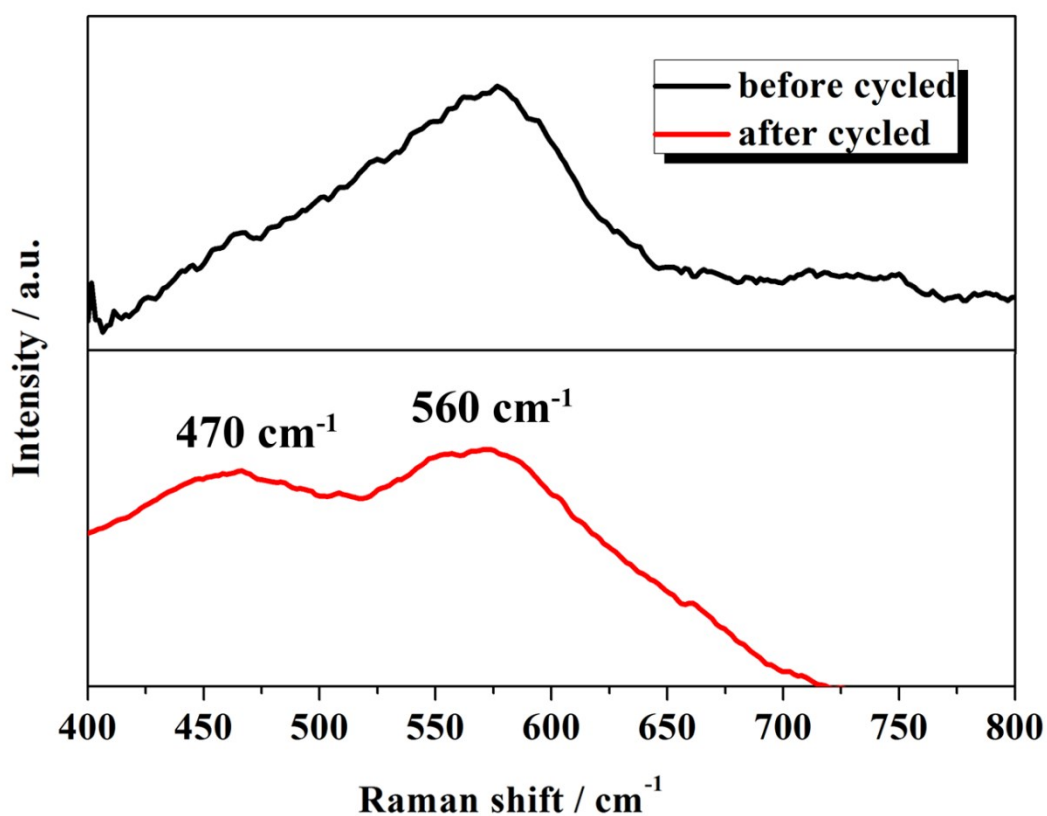


**Fig. S5** Raman spectra of 3D-NA/NiZn-phytate before and after cycled.

Besides, the Raman spectra before and after cycled are contrasted in Fig. S5. Notably, the typical Raman peak for Ni-O vibration has been divided into two isolated peaks after 1000 cycles, revealing the generation of Ni(OH)<sub>2</sub> (470 cm<sup>-1</sup>) and NiOOH (560 cm<sup>-1</sup>) with disordered or defective form.<sup>3,4</sup>

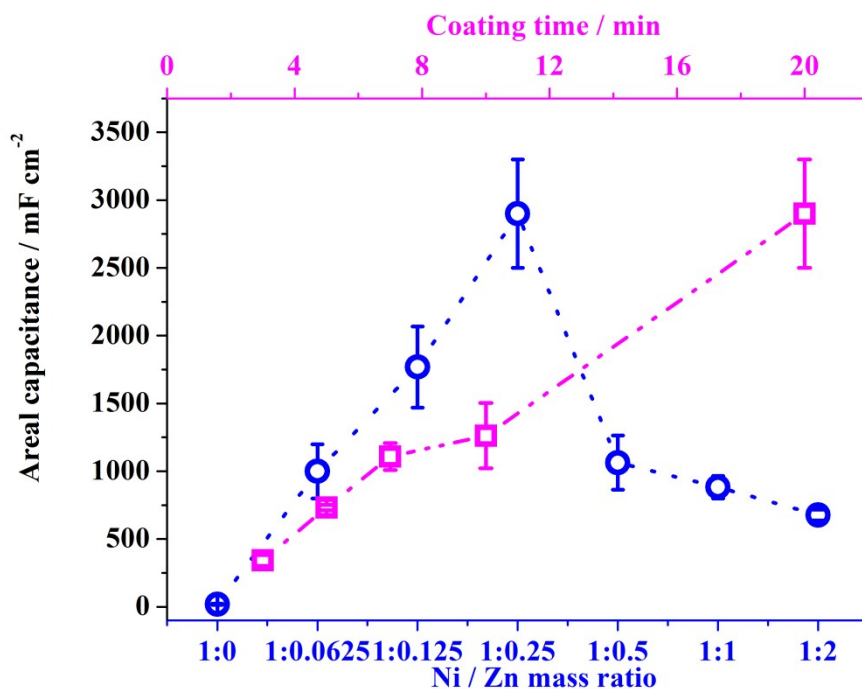


**Fig. S6** Areal capacitance (obtained at the current density of  $10 \text{ mA cm}^{-2}$  in  $6 \text{ M KOH}$ ) of 3D-NA/NiZn-phytate prepared at various conditions, including coating time ranged from 3 to 20 min (purple rectangles, Ni/Zn mass ratio is fixed at 1:0.25) and plating solution with different Ni/Zn mass ratio (blue circles, coating time is fixed at 20 min).

As shown in Fig. S6 (marked with purple rectangles), the areal capacitance (obtained at the current density of  $10 \text{ mA cm}^{-2}$  in  $6 \text{ M KOH}$ ) is improved with prolonging the coating time. Combined with Table S3, we also notice that the mass of active materials steadily increases along with the increment of coating time, which can well explain the uphill trend in Fig. S6. While, the coating time reaching to 20 min, the active material mass is up to  $\sim 1.0 \text{ mg}$  considered as the meaningful mass loading for the supercapacitors.<sup>5</sup> As for the study of the plating solution, the electrodes, prepared in several plating solution with different Ni/Zn mass ratio, are measured with GCD curves at the current density of  $10 \text{ mA cm}^{-2}$  in  $6 \text{ M KOH}$  to obtain the according areal capacitance in Fig. S6 (marked with blue circles). From the presentation here, the tendency of this curve grows with the increment of Zn content in plating solution, but declines with the further addition of Zn moiety. To interpret this phenomenon, component analysis of as-fabricated 3D-NA/NiZn substrate in different plating solution is conducted via the EDS measurements in Table S4. As indicated here, the variation of Ni and Zn contents on 3D-NA/NiZn is associated with the change in these of plating solution, where a dramatic change in the mass percentage is observed from Ni/Zn = 1:0.125 to 1:0.25. Meanwhile, there is the considerable areal capacitive change found in this region from Fig. S6, suggesting Ni and Zn contents in active plating layer show essential effects on capacitive performances.

**Table S3** Active materials mass loading on 3D-NA at various coating time.

Coating time*	Active materials mass loading (mg cm <sup>-2</sup> )
3	≅ 0.10
5	≅ 0.10
7	0.47
10	0.62
20	1.15

\*the mass per square centimeter is obtained by the weight difference between the substrate (3D-NA) and the electrode at the fixed condition and the final values are generally the average of 5 individual electrodes.

**Table S4** Weight percentage (determined by EDS analysis) of Ni and Zn of 3D-NA/NiZn-phytate electrodes prepared in different plating solution with specific Ni/Zn mass ratio.

Ni/Zn	Ni (Wt%)	Zn (Wt%)
1:0	100	0
1:0.0625	64.22	35.78
1:0.125	53.23	46.77
1:0.25	10.25	89.75
1:0.5	9.11	90.89
1:1	6.87	93.13
1:2	5.66	94.34

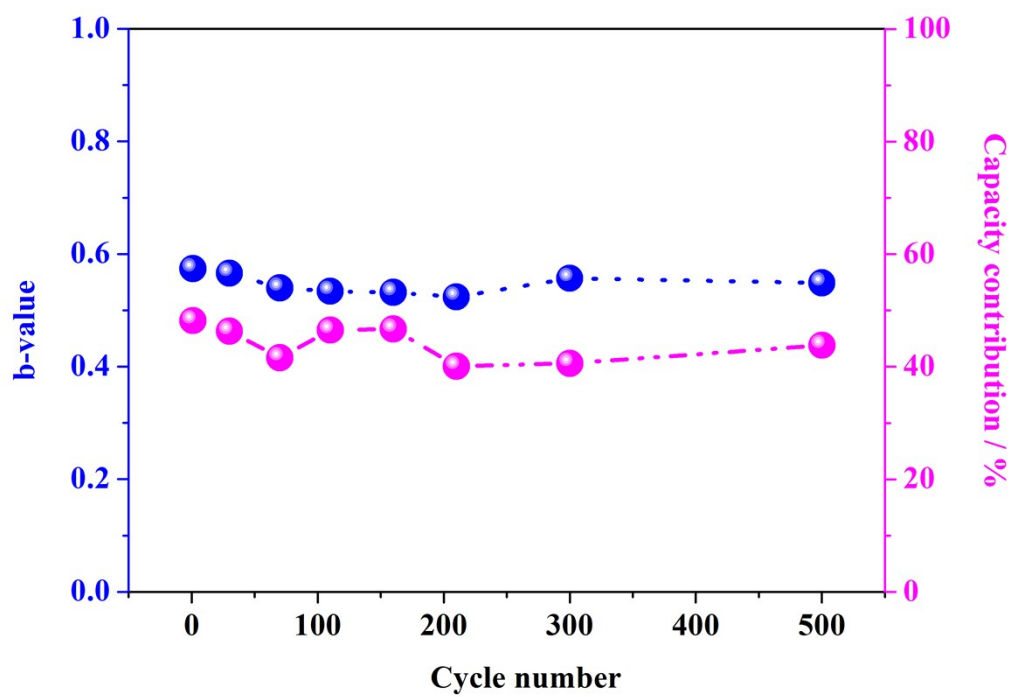


**Fig. S7** b-value (blue) and capacitive contribution (purple) of 3D-NA/NiZn-phytate electrode at different cycles.

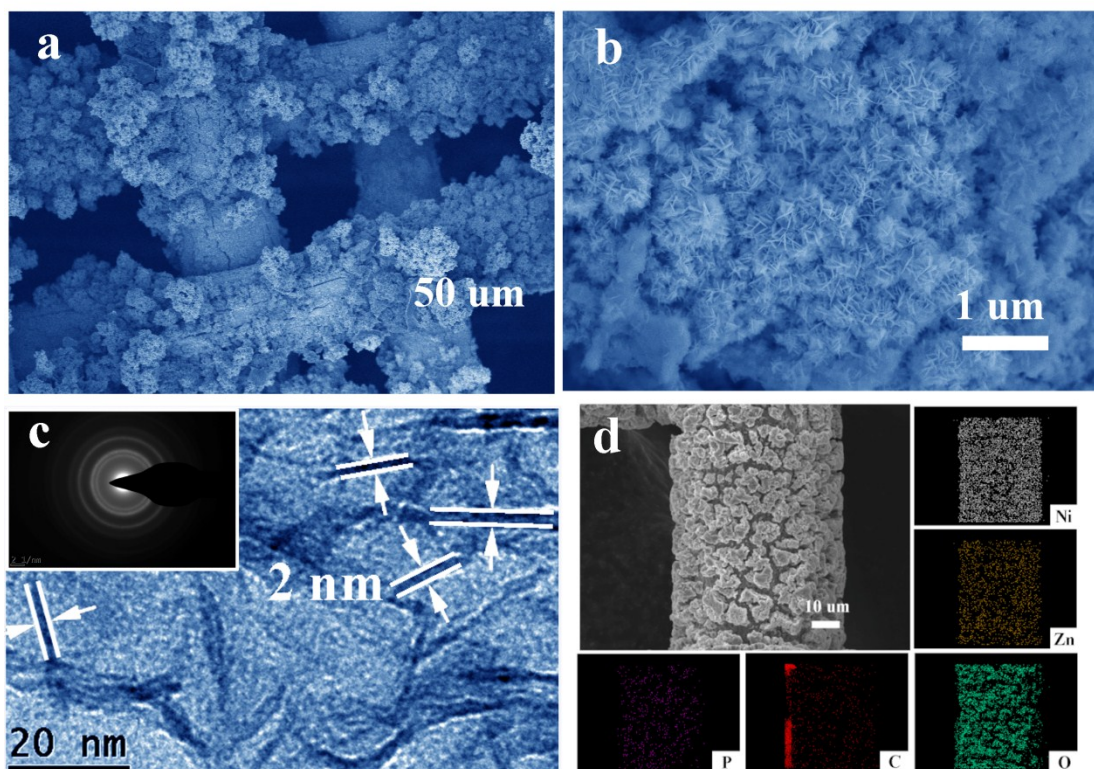


**Fig. S8** SEM images (a, b), TEM (c), SAED pattern (the inset of c) and EDS mapping (d) of 3D-NA/NiZn-phytate after 500 cycles.

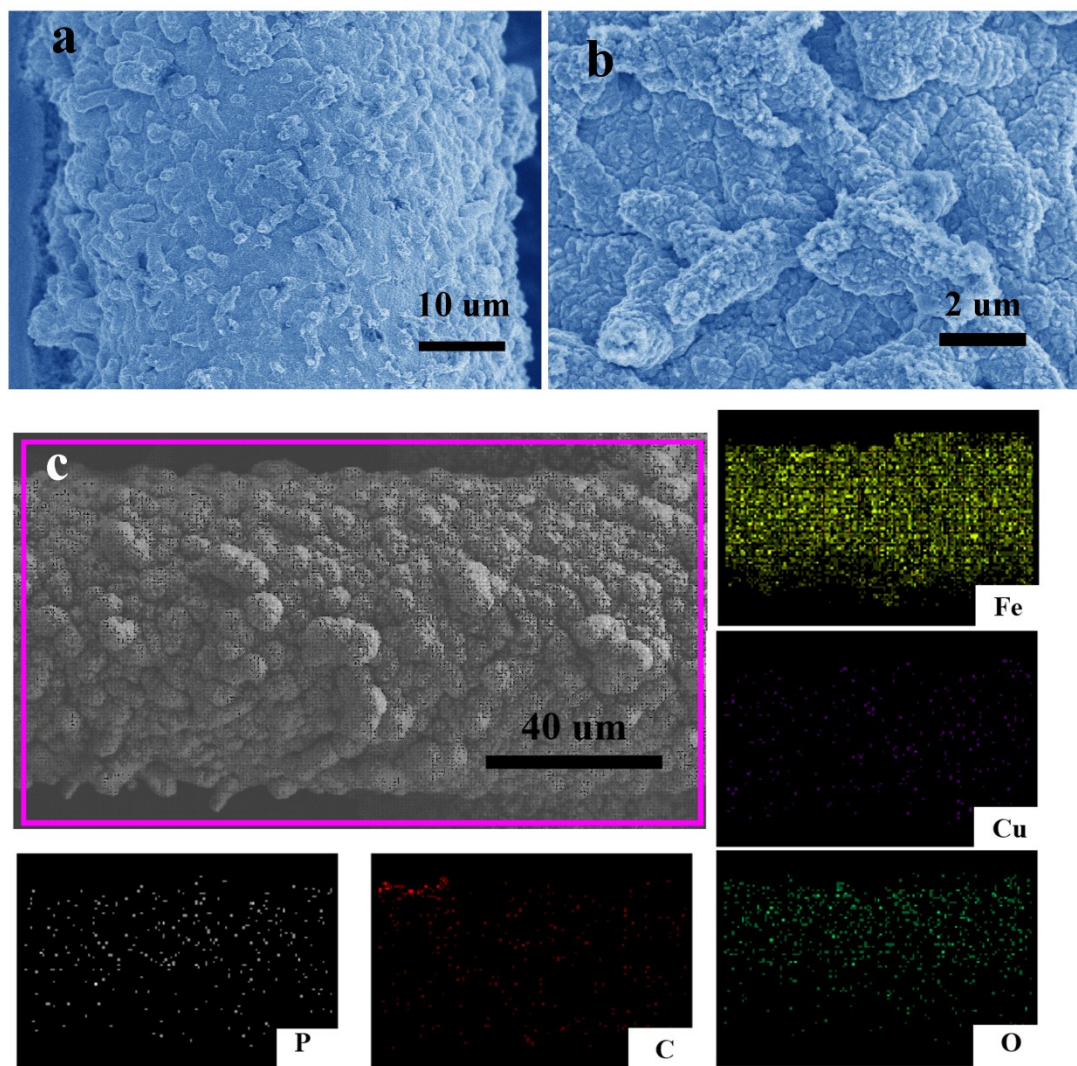


**Fig. S9** SEM images (a, b) 3D-NA/Fe and EDS mapping of 3D-NA/Fe-phytate.

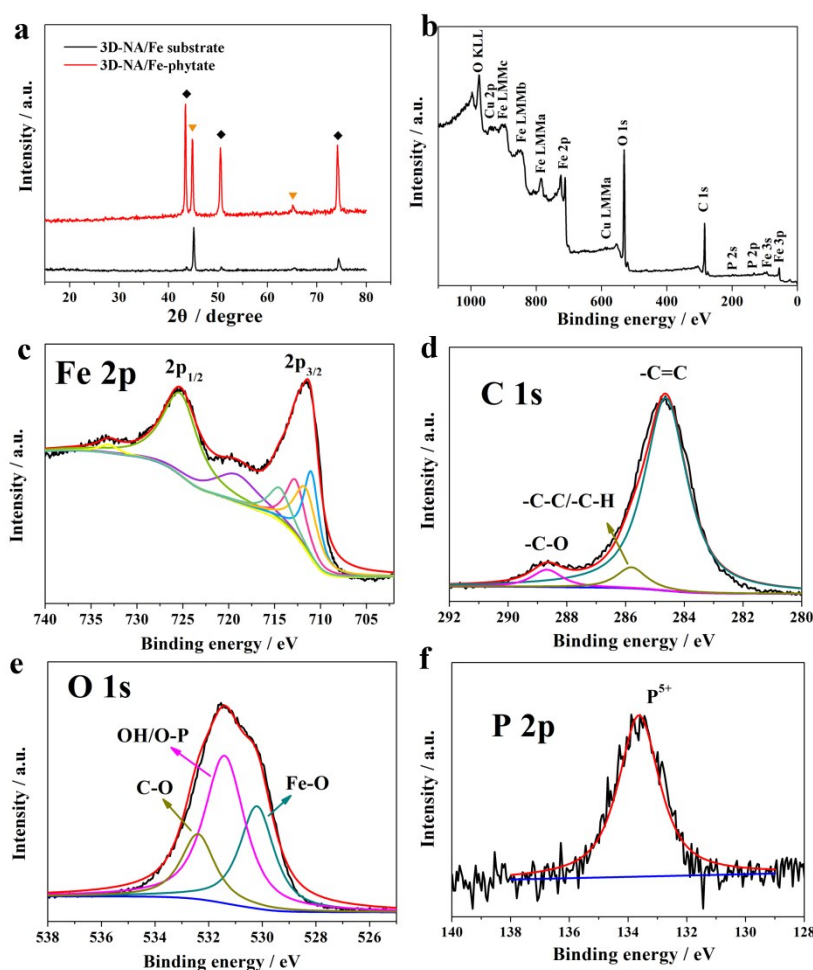


**Fig. S10** XRD pattern of 3D-NA/Fe and 3D-NA/Fe-phytate (a); survey scan XPS of 3D-NA/NiZn-phytate before cycled (b) and the relative Fe 2p (c), C 1s (d), O 1s (e) and P 2p (f) spectra.

Next, the visualized element composition of 3D-NA/Fe-phytate electrode surface is studied through the element mapping. From Fig. S9c, every element has been filled with the individual color and the color intensity shows the element content. As a result, the major element is Fe, while the other elements, including P, C and O, is detected with less contents and all the elements are equally distributed on the electrode surface. Moreover, the XRD pattern of 3D-NA/Fe substrate indicates that the majority constituent is metallic iron according to a strong peak at around 45 degree and a minor peak at approximate 65 degree (marked with ▼ in Fig. S10a).<sup>5</sup> On the contrary, other peaks belonging to Cu substrate (marked with ◆ in Fig. S10a) is not significant. This is mainly because the thick Fe coating on the surface can block diffracted signal of Cu substrate. When the 3D-NA/Fe substrate is treated with phytic acid to form 3D-NA/Fe-phytate, the electrode shows the enhanced diffracted intensity of Cu. The reason for this change should be that the strong corrosion and coordination abilities enable phytic acid to react with metallic Fe and further dissolve the great amount of Fe, after which Cu substrate can be exposed.



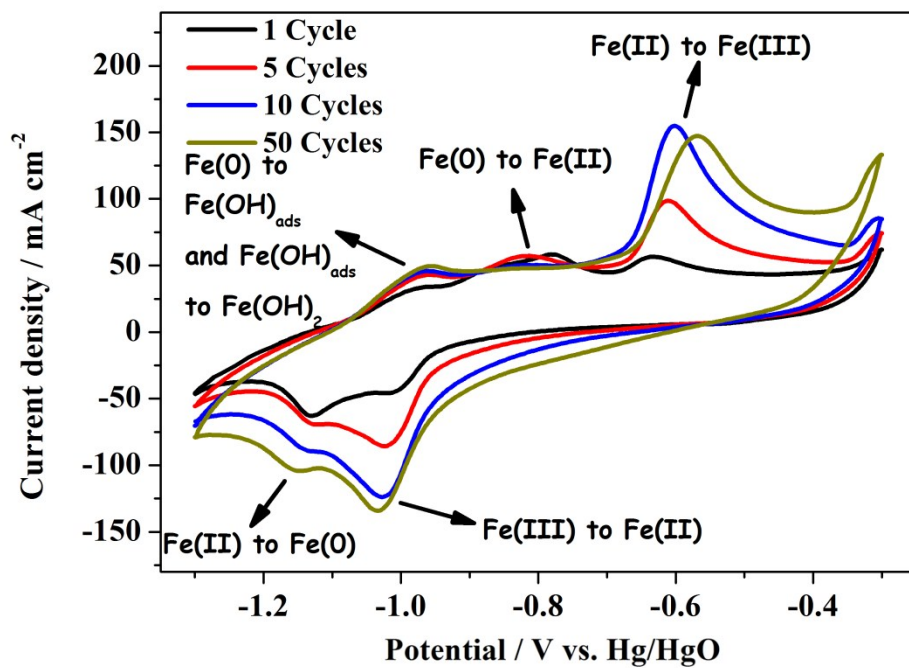


**Fig. S11** Initial CV curves of the 3D-NA/Fe-phytate electrode in 6M KOH at the scan rate of 50 mV s<sup>-1</sup>.

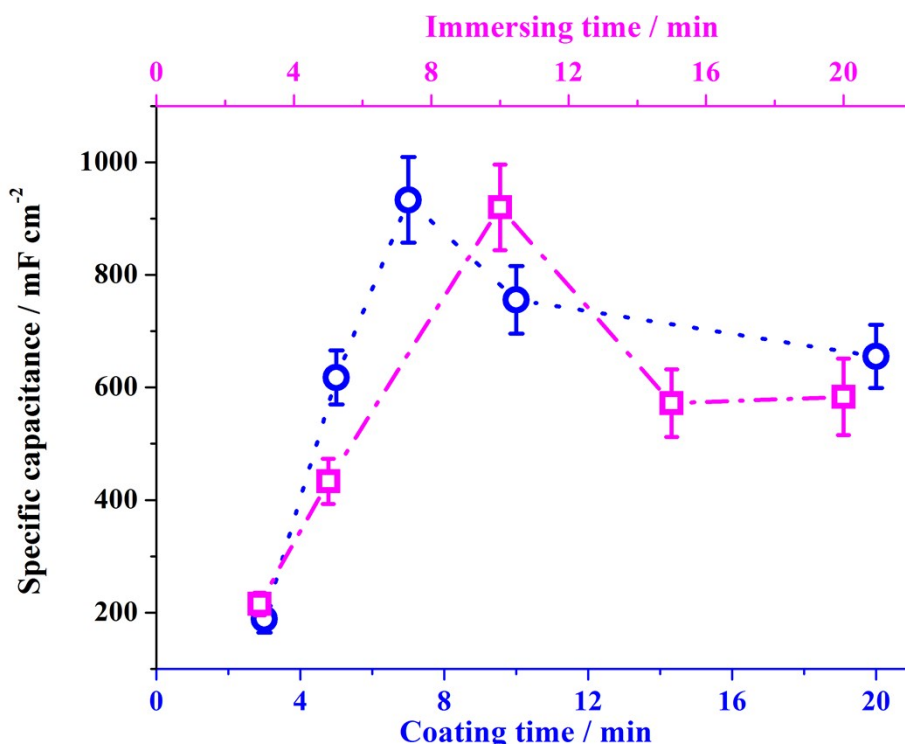


**Fig. S12** Specific capacitance (obtained at the current density of  $10 \text{ mA cm}^{-2}$  in  $6 \text{ M KOH}$ ) of 3D-NA/Fe-phytate prepared at various conditions, including coating time ranged from 3 to 20 min (blue circle, immersing time is fixed at 10 min) and immersing time in phytic acid solution (purple rectangle, coating time is fixed at 7 min).

As shown in Fig. S12 (blue circle), specific capacitance of 3D-NA/Fe-phytate electrode (immersing time is fixed at  $\sim 10 \text{ min}$ ) reveals an upward trend along with the increased coating time at the first 7 min, while, after which time, it decreases. This is probably because prolonging coating time can induce the increment of the thickness of iron plating, further leading to the poor electron transfer from the electrode surface to the substrate. The areal capacitance also sees the similar tendency in the investigation of coating time. There is a dramatic growth of capacitance at the first several minutes in Fig. S12 (purple rectangle), then the value peaks at 10 min. After that, the increased immersing time can cause the substantial drop of performance, which is possibly ascribed to considerably declined mass of active materials at excessively long immersion time in phytic acid.

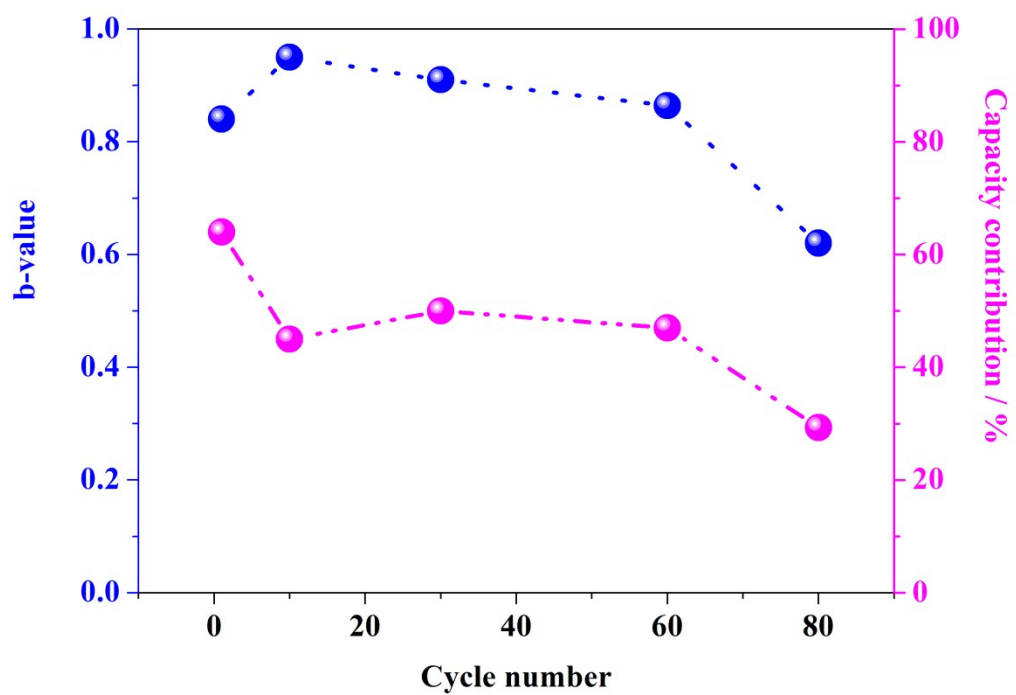


**Fig. S13** b-value (blue) and capacitive contribution (purple) of 3D-NA/Fe-phytate electrode at different cycles.

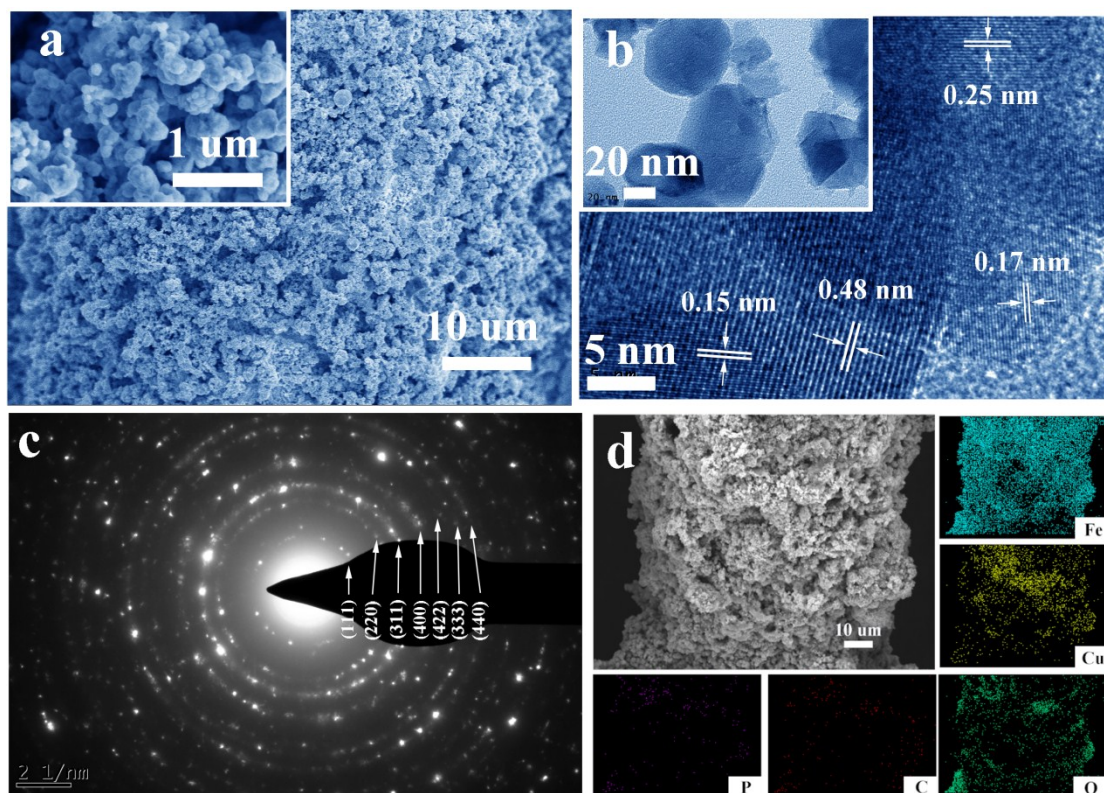


**Fig. S14** SEM images (a), TEM (b), SEAD pattern (c) and EDS mapping (d) of 3D-NA/Fe-phytate after 500 cycles.

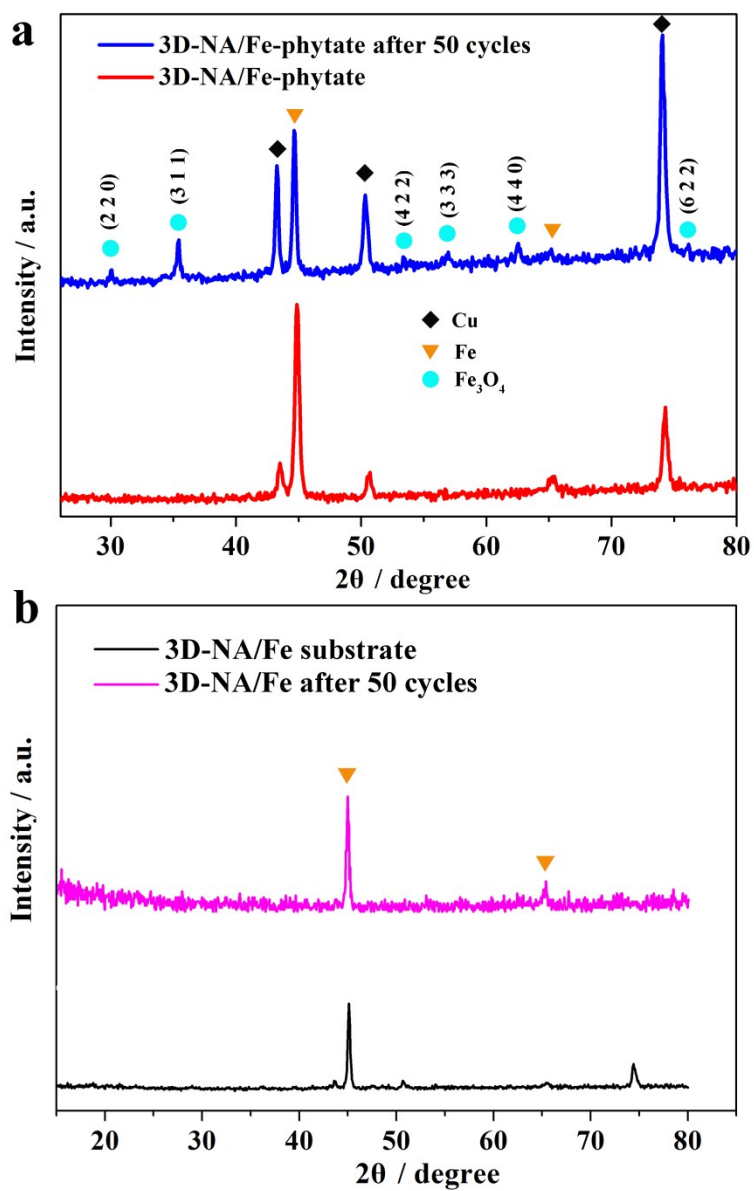


**Fig. S15** XRD patterns of 3D-NA/Fe-phytate (a) and 3D-NA/Fe (b) before and after 50 cycles.

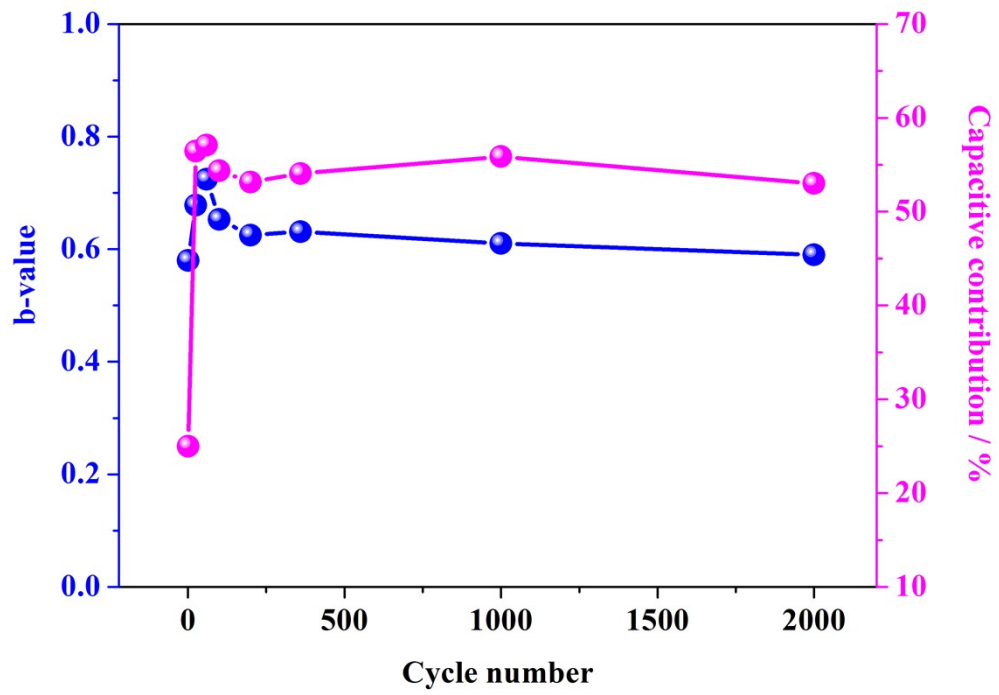


**Fig. S16** b-value and capacitive contribution of Ni/Fe full cell at different cycles.

## The determination of electrochemical performances in this work.

**Specific capacitance ( $C_s$ , F g<sup>-1</sup>) and mass capacity ( $C_m$ , mAh g<sup>-1</sup>) based on the mass of active materials.** The  $C_s$  and  $C_m$  of electrodes calculated from galvanostatic charge-discharge measurements using the following equations:

$$C_s = \int I_m dt / V$$

$$C_m = \int I_m dt / 3600$$

where  $I_m$  (A g<sup>-1</sup>) is the current density (according to the mass of active materials) applied to the electrode,  $V$  (V) is the working potential window,  $dt$  (s) is time differential of discharge process.

**Energy density.** The energy density ( $E$ , Wh kg<sup>-1</sup>) is obtained according the following formula:

$$E = \int I_m V dt / 1000$$

where  $I_m$  (A g<sup>-1</sup>) is the current density (according to the mass of active materials) applied to the electrode,  $V$  (V) is the working potential window,  $dt$  (s) is time differential of discharge process.

**Power density.** The power density ( $P$ , kW kg<sup>-1</sup>) is calculated based on the equation as follows:

$$P = E / \Delta t$$

where  $E$  (Wh kg<sup>-1</sup>) is the energy density and  $\Delta t$  (s) is the discharging time.

**b-value.** The relationship between peak currents and scan rates obey the following equation:

$$i = av^b$$

where  $i$  is peak current,  $v$  is scan rate,  $a$  and  $b$  are adjustable parameters and  $b$ -values are determined from the slope of the plot of  $\log i$  vs  $\log v$ . For  $b = 0.5$ , the current response is diffusion-controlled (faradaic intercalation process); for  $b = 1.0$ , it is indicative of a capacitive response (non-faradaic process).

**Capacitive contribution.** The capacitive contribution is calculated via the Dunn's method as follows:

$$i(V) = k_1 v + k_2 v^{1/2}$$

in which the total current density ( $i$ ) at a fixed potential ( $V$ ) is contributed by the current response of surface capacitive effects ( $k_1 v$ ,  $v$  is the scan rate) and diffusion-controlled insertion processes ( $k_2 v^{1/2}$ ).

This equation can be transformed to be:

$$\frac{i(V)}{v^{1/2}} = k_1 v^{1/2} + k_2$$

Therefore, values of  $k_1$  and  $k_2$  can be calculated according to the plot of  $i(V)/v^{1/2}$  vs.  $v^{1/2}$ . Then, each part of current density can be separated.

## References

1. P. P. Li, Z. Y. Jin, J. Yang, Y. Jin and D. Xiao, *Chem. Mater.*, 2016, **28**, 153-161.
2. P. P. Li, Z. Y. Jin, R. Wang, Y. Jin and D. Xiao, *J. Mater. Chem. A*, 2016, **4**, 9486-9495.
3. M. W. Louie and A. T. Bell, *J. Am. Chem. Soc.*, 2013, **135**, 12329-12337.
4. M. Merrill, M. Worsley, A. Wittstock, J. Biener and M. Stadermann, *J. Electroanal. Chem.*, 2014, **717**, 177-188.
5. H. Wang, Y. Liang, M. Gong, Y. Li, W. Chang, T. Mefford, J. Zhou, J. Wang, T. Regier, F. Wei and H. Dai, *Nat. Commun.*, 2012, **3**, 917-924.